Chemical forms of calcium in Ca,Zn- and Ca,Cd-containing grains excreted by tobacco trichomes[1]

Géraldine Sarret, Marie-Pierre Isaure, Matthew A. Marcus, Emiko Harada, Yong-Eui Choi, Sébastien Pairis, Sirine Fakra, and Alain Manceau

Abstract: Tobacco (*Nicotiana tabacum* L. cv. Xanthi) plants exposed to toxic levels of zinc and cadmium excrete metals through their leaf trichomes (epidermal hairs) as Zn,Ca- and Cd,Ca-containing grains. Little is known about the nature and formation mechanism of these precipitates. The chemical, crystalline, and noncrystalline compositions of individual grains produced by tobacco were studied by scanning electron microscopy coupled with energy dispersive X-ray analysis (SEM-EDX), micro-X-ray diffraction (µXRD), and calcium K-edge micro X-ray absorption near edge structure (µXANES) spectroscopy. Zinc is predominantly incorporated in calcite and cadmium in calcite and vaterite. Aragonite, which occurs occasionally, does not seem to contain trace metals. In addition to being precipitated in its three possible polymorphic forms, calcite, aragonite, and vaterite, calcium is also speciated as amorphous $CaCO_3$ and possibly organic Ca in some grains. Most often, a particular grain consists of two or more crystalline and noncrystalline phases. The observed variability of intra- and inter-grain elemental and phase composition suggests that this biomineralization process is not constrained by biological factors but instead results from thermodynamically and kinetically controlled reactions. This study illustrates the potential of laterally resolved X-ray synchrotron radiation techniques (µXRD and µXANES) to study biomineralization and metal immobilization processes in plants.

Key words: biomineralization, detoxification, micro-XANES, micro-XRD.

Résumé : Lorsque des plants de tabac (*Nicotiana tabacum* L. cv. Xanthi) sont exposés à des niveaux toxiques de zinc et de cadmium, ils excrètent des métaux par les trichomes (poils épidermiques) de leurs feuilles qu'on retrouve sous la forme de grains contenant du Zn,Ca et du Cd,Ca. On connaît peu de choses sur la nature et le mécanisme de formation de ces précipités. On a étudié les compositions chimiques cristallines et non cristallines de grains individuels produits par le tabac en faisant appel à la microscopie électronique à balayage couplée à l'analyse des rayons X en dispersion d'énergie (MEB-XDE), à la diffraction micro des rayons X (µDRX) et à la micro spectroscopie d'absorption X de type XANES (µXANES) au seuil *K* du calcium. Le zinc est principalement incorporé dans la calcite et le cadmium dans la calcite et la vatérite. L'aragonite qu'on rencontre occasionnellement ne semble pas contenir de traces de métaux. En plus d'être précipité sous ses trois polymorphes possibles, calcite, aragonite et vatérite, le calcium se trouve aussi sous la forme de $CaCO_3$ amorphe et possiblement sous la forme de Ca organique dans certains grains. Le plus souvent, un grain est formé d'au moins deux phases cristallines et non cristallines. La variabilité tant intra- qu'intergrains en terme de composition élémentaire et de nature des phases suggère que ce processus de biominéralisation n'est pas contraint par des facteurs biologiques, mais qu'il résulte plutôt de réactions sous contrôle thermodynamique et cinétique. Cette étude illustre le potentiel des techniques de rayonnement X synchrotron résolues latéralement (µDRX et µXANES) dans l'étude des processus de biominéralisation et d'immobilisation des métaux dans les plantes.

Mots-clés : biominéralisation, détoxification, spectroscopie d'absorption micro-X de type XANES (µXANES), diffraction micro des rayons X (µDRX).

[Traduit par la Rédaction]

G. Sarret,[2] M.-P. Isaure, E. Harada, and A. Manceau. Environmental Geochemistry Group, LGIT, University of Grenoble and CNRS, BP 53, 38041 Grenoble cedex 9, France.
M.A. Marcus and S. Fakra. Advanced Light Source (ALS), Lawrence Berkeley National Lab, MS 6–100, Berkeley, CA 94720, USA
E. Harada and Y.-E. Choi. Division of Forest Resources, College of Forest Sciences, Kangwon National University, Chunchon 200–701, Kangwon-do, Korea.
S. Pairis. Institut Néel CNRS-UJF, Dept. Matière Condensée, Matériaux et Fonctions, Pôle Instrumentation (Microscopie Electronique), 25 av. des Martyrs, BP 166, 38042 Grenoble cedex 9, France.

Table 1. Tobacco culture conditions and name of the grains investigated.

Treatment conditions	Cation concentrations in the nutrient solution (mmol/L)			Grain names	Techniques and references				
	Ca	Zn	Cd		SEM-EDX	µXRD	Zn µEXAFS	Cd µXANES	Ca µXANES
Zn	0.28	0.25	0	Zn2	(3) and this work	(3)	(3)	—	This work
				Zn3	—	This work	Unpublished	—	This work
Zn + Ca	3.28	0.25	0	ZnCa3	(3) and this work	(3)	(3)	—	This work
				ZnCa4	(3) and this work	(3)	(3)	—	This work
				ZnCa5	—	This work	Unpublished	—	This work
Cd	0.28	0.08×10^{-3}	0.025	Cd10	See footnote a	See footnote a		See footnote a	This work
Cd + Ca	3.28	0.08×10^{-3}	0.025	CdCa2	See footnote a	See footnote a		See footnote a	This work
				CdCa3	See footnote a	See footnote a		See footnote a	This work
				CdCa6	See footnote a	See footnote a		See footnote a	This work
Ca	3.28	0.08×10^{-3}	0	Ca3	This work	—	—	—	—

aIsaure et al., manuscript in preparation.

Introduction

Recently, a novel original mechanism of Zn and Cd detoxification was described in tobacco (*Nicotiana tabacum* L. cv. Xanthi). Tobacco exposed to Cd excreted Cd,Ca-containing grains through leaf trichomes (1, 2), and a similar excretion of Zn,Ca-containing grains was observed under Zn exposure (3). Trichomes are specialized epidermal structures. In tobacco, they are glandular and excrete various organic substances including nicotine and resins. This detoxification process may have implications in human health, since smoking is one of the principal routes of exposure to heavy metals, and also in phytoremediation as tobacco is a candidate species for phytoextraction.

The morphology, elemental composition, mineralogy, as well as Zn and Cd speciation in the grains were investigated by scanning electron microscopy coupled with energy dispersive X-ray analysis (SEM-EDX), micro-X-ray fluorescence (µXRF), micro-X-ray diffraction (µXRD), Zn K-edge micro extended X-ray absorption fine structure (µEXAFS) (3), and Cd L_{III} edge micro X-ray absorption near edge structure (µXANES) spectroscopy (Isaure et al., manuscript in preparation). Calcium was always the major component. µXRD analyses revealed the presence of calcite and less frequently vaterite and aragonite, two other $CaCO_3$ polymorphs. Calcium oxalate mono- and di-hydrate were occasionally found. Calcite and vaterite were substituted by cations, probably Zn, Cd, and possibly Mn and Mg. Zn µEXAFS confirmed the occurrence of Zn-substituted calcite and evidenced Zn associations with other phases including organic compounds, silica, and phosphate (3). Cd µXANES showed that cadmium was a Ca substituent in calcite and vaterite and (or) sorbed on the surface of these minerals (Isaure et al., manuscript in preparation).

The mechanism of formation of these grains remains unclear. Biogenic minerals may result from a controlled biomineralization process leading to well-defined minerals and shapes. They may also be biologically induced, which means that an organism promotes the precipitation but does not control the crystallization process (4). In the present case, grains could result from the exudation of a liquid containing the various metals and substances and the precipitation of the various solid phases because of water evaporation. Alternatively, they might be formed intracellularly and excreted thereafter as suggested by Choi and Harada (5). The purpose of this study is to better characterize the structure and composition of the grains. Grains excreted by tobacco, under various Zn, Cd, and Ca exposure conditions, were investigated by SEM-EDX, µXRD, and Ca K-edge µXANES spectroscopy. Results of these complementary approaches are compared, and a hypothesis for the formation of the grains is proposed in light of these data.

Experimental

Materials

Plant culture and grain collection procedures have been described previously (3). Briefly, tobacco plants were grown in hydroponic conditions and exposed for 5 weeks to Zn or Cd, with or without a supplement of Ca (Table 1). A control condition with Ca only was also tested. Then, grains were

collected by washing the leaves in ultrapure water and centrifugating the suspension. Several Ca-containing reference compounds were used for the Ca XANES data analysis. Calcite, vaterite, and Cd-containing vaterite were synthesized at room temperature (RT) according to a modified protocol of Paquette and Reeder (6, 7). Briefly, an aqueous solution (500 mL) containing 10 mmol/L $CaCl_2$ and 1.8 mol/L NH_4Cl was placed in a glass reactor, an EPPENDORF tube containing solid ammonium carbonate was allowed to float at the surface of the solution, and the reactor was closed and kept unstirred. NH_4Cl was used as a background electrolyte to provide a high ionic strength. Initial pH was 4.9. The decomposition of ammonium carbonate produces $NH_3(g)$ and $CO_2(g)$, which dissolve into the solution simultaneously increasing pH and alkalinity. The supersaturation of the solution induces the formation and growth of $CaCO_3$ crystals. Continuous sublimation of $NH_3(g)$ buffers the solution around pH = 7.9. After 13 days, the reactor contained rhombohedral crystals and spherical particles attached to the surface of the glass. The two types of particles were separated and characterized by XRD. Rhombohedral crystals corresponded to calcite and spherical particles to vaterite. For the synthesis of Cd-containing vaterite, the same procedure was used except that after 13 days, when crystal size amounted to 150–200 μm in diameter, the $CaCl_2$–NH_4Cl solution was progressively doped with 0.1 mol/L $CdCl_2$ to a total concentration of 100 μmol/L Cd to incorporate Cd as a Ca substituent in vaterite (6, 7). The progressive addition of $CdCl_2$ kept the solution undersaturated with respect to otavite ($CdCO_3$). After 7 days, the particles were collected and separated. Spherical particles were identified as Cd-containing vaterite by XRD and μXRF. The Cd content was 1–20 ppm based on μXRF analysis.

Aragonite was a natural specimen. The XANES spectrum for synthetic amorphous $CaCO_3$ was provided by Y. Politi (8). Ca oxalate monohydrate (whewellite) was purchased from Sigma-Aldrich. A solution containing 0.5 mol/L $Ca(NO_3)_2$ at pH 2.6 was used as a reference for aq. Ca^{2+}. The phase purity of all crystalline samples was checked by XRD prior to XANES analysis.

Electron microscopy

The morphology and the chemical composition of the grains were studied by SEM-EDX using a Jeol-JSM 840A equipped with a Kevex Si(Li) detector. The chamber pressure was 10^{-6}–10^{-5} torr (1 torr = 133.322 4 Pa), and the accelerating voltage was 20 kV. Grains were mounted on kapton tape or on carbon tape, then fixed on carbon stubs and coated with carbon. Images were taken at a magnification of 500 to 10 000. EDX spectra were recorded on prominent spots of the grains to optimize the detection.

μXRF, μXRD, and μXANES

The μXRF, μXRD, and Ca K-edge μXANES measurements were performed on beamline 10.3.2 of the Advanced Light Source (ALS, Berkeley, California) (9). The grains were spread on kapton tape and analyzed at RT and pressure. First, each grain was mapped by μXRF. Then, μXANES and μXRD data were recorded on the Zn-richest region for the Zn and Zn + Ca treatments, on the Cd-

richest region for the Cd and Cd + Ca treatment, and on the Ca-richest region for the Ca treatment. μXRF data were collected at 10 keV with a beam size of 5 × 5 μm. The same X-ray spot size was used for Ca μXANES. Fluorescence X-ray yield was measured with a 7-element Ge solid-state detector. The spectra were recorded between 3900 to 4400 eV. μXRD patterns were recorded at an incident energy of 17 keV with a beam size of 16 × 7 μm. More experimental details are given in (3). Ca XANES reference spectra were recorded at RT on beamline ID21 at the European Synchrotron Radiation Facility (ESRF, Grenoble, France). Each spectrum is the average of two to three spectra, each about 15 min long.

XRD and XANES data treatment

The XRD data treatment was performed as described previously (3). Briefly, after calibration with alumina, two-dimensional XRD patterns were integrated to one-dimensional patterns for peak assignment. For substituted calcite crystals the unit cell parameters a and c were refined, and the stoichiometry of the substituent was estimated from these two parameters using the Vegard law (10) with calcite, smithsonite ($ZnCO_3$), and otavite ($CdCO_3$) as end members for the Ca-Zn and Ca-Cd solid solutions. This approach cannot be used for substituted vaterite because of the absence of a $CdCO_3$ structural analogue of vaterite.

XANES spectra were processed using WinXAS (11). All spectra were energy-calibrated with respect to calcite (the inflection point for this reference was set to 4042.6 eV). The collected scans were averaged; the background was subtracted and normalized using linear (pre-edge) or cubic (post-edge) polynomials. XANES spectra were then fitted by linear combinations using calcite, aragonite, vaterite, Cd-containing vaterite, amorphous $CaCO_3$, aq. Ca^{2+}, and Ca oxalate monohydrate reference spectra. The quality of the fits was quantified by the normalized sum-squares residuals NSS = $\sum(\mu_{experimental} - \mu_{fit})^2 / \sum(\mu_{experimental})^2 \times 100$, in the 4000–4150 eV range, where μ is the normalized absorbance. An energy shift of ±0.5 eV maximum and a correction of slope were allowed to account for the energy resolution of the monochromator and for possible inconsistencies in data processing. For some spectra, linear combination (LC) fitting did not provide satisfactory results, and over-absorption effects were suspected based on the comparison of these spectra with the standards. Therefore, each spectrum was fitted with and without a correction of over-absorption using a simple model (12). This model assumes that the smooth part of the resonant absorption is a constant fraction of the nonresonant background (which is a reasonable assumption in the XANES region), and that the sample is infinitely thick, i.e., totally absorbs the incident beam (which is probably true considering the energy range and the size and global composition of the grains). The equation used is,

[1] $\qquad y_{experimental} = (1 + a) / (1 + ay_{corrected})$

where y is the normalized resonant absorbance (which equals 0 below the edge and oscillates around 1 above the edge) and $a = \mu_{resonant} / (\mu_{nonresonant} + \mu_{fluorescence})$, where $\mu_{resonant}$, $\mu_{nonresonant}$, and $\mu_{fluorescence}$ are the three components of the absorbance μ.

Equation [1] can be solved as,

Fig. 1. SEM imaging for the grains (*a*) ZnCa3, (*b*) ZnCa4, (*c*) Zn2, (*d*) CdCa3, and (*e*) Ca3. EDX analyses were performed on the spots marked by a black cross.
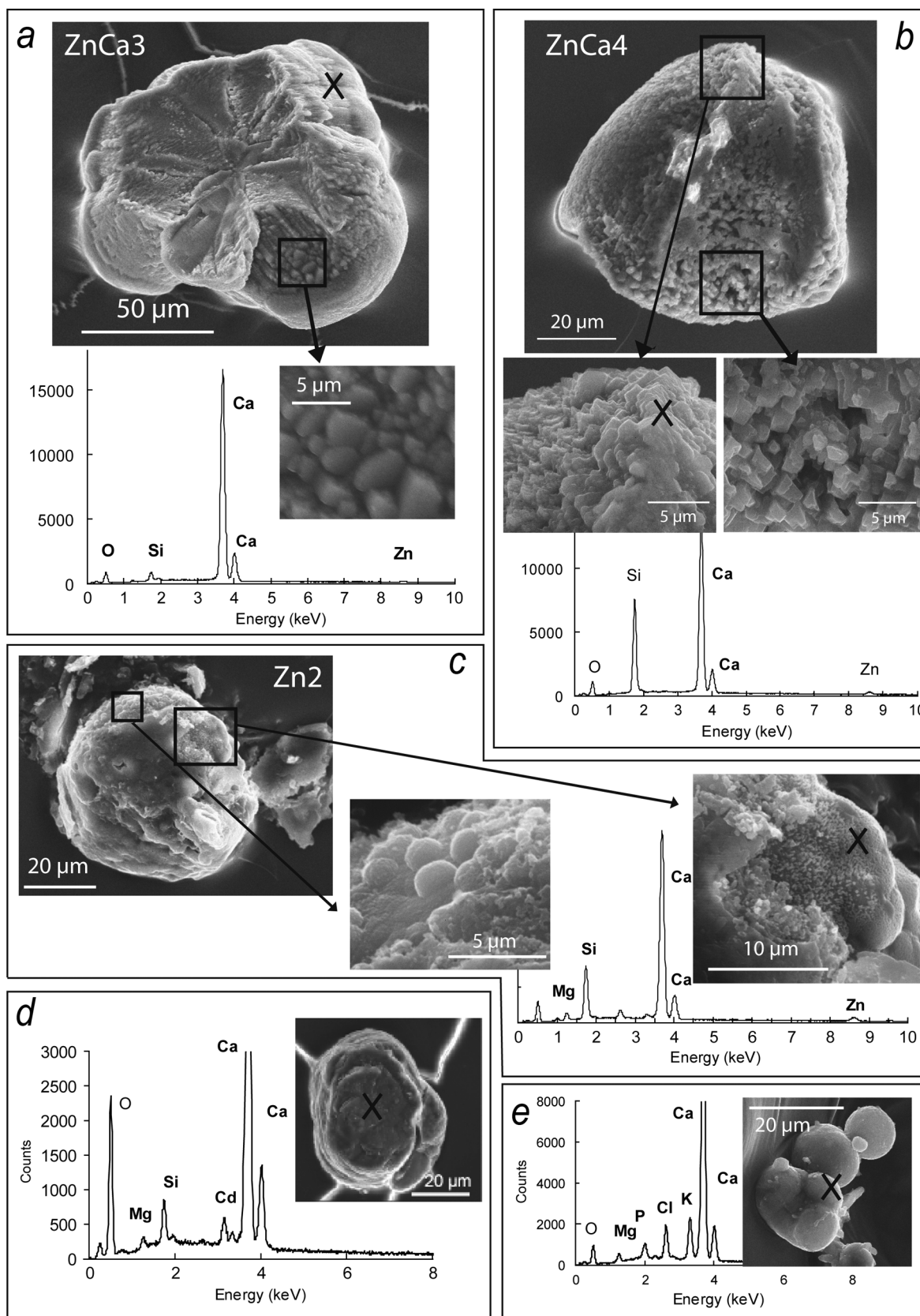
Fig. 2. (*a*) μXRF spectrum and (*b*) one- and two-dimensional μXRD patterns for grains ZnCa5 and Zn3. All XRD peaks were attributed to substituted calcite. The positions of three peaks for pure calcite are indicated by arrows.
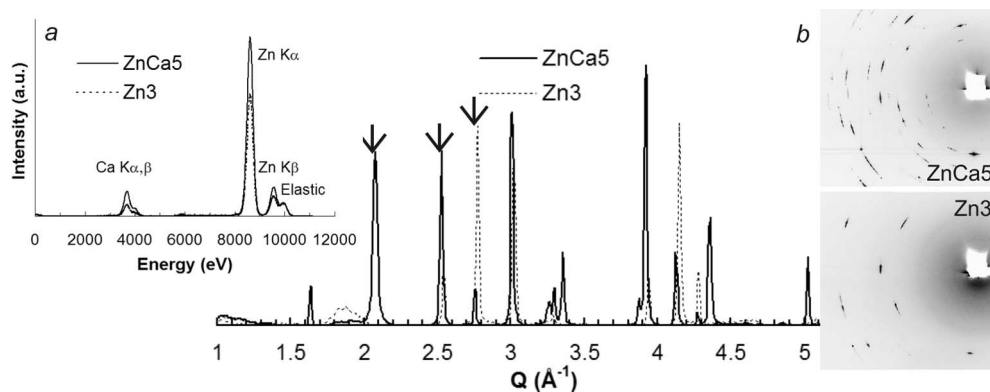
[2] $\qquad y_{corrected} = y_{experimental} / (1 + a(1 - y_{experimental}))$

The over-absorption parameter *a* equals 0 in the absence of an over-absorption effect and increases with this effect. Because of the sample heterogeneity, the precise composition of the sample is not known, so *a* is an adjusted parameter.

Results

The morphology of the grains as observed by SEM varied considerably. The grains varied from 10 to 150 μm in diameter. Each grain is an aggregate of different types of particles. The first type is composed of micro-faceted crystallites (insets in Figs. 1*a* and 1*b*), and the second type is composed of globular structures of various sizes (from 2 to 50 μm, see Figs. 1*c*–1*e*). Some grains such as Zn2 (Fig. 1*c*) seem visually less crystalline. The elemental composition of the grains varies from one grain to another and within the same grain. Ca was always the major component regardless of the plant metal treatment conditions. Minor elements include Mg, Si, P, Cl, K, and Zn or Cd depending on the plant treatment (Fig. 1). The high Si peaks observed in Figs. 1*a*–1*d* are attributed to kapton tape on which the grains were mounted. Silicon is not detected in the grain presented in Fig. 1*e* (mounted on carbon tape). However, Si was found in small amounts in some grains (not presented in this study), as was Mn.
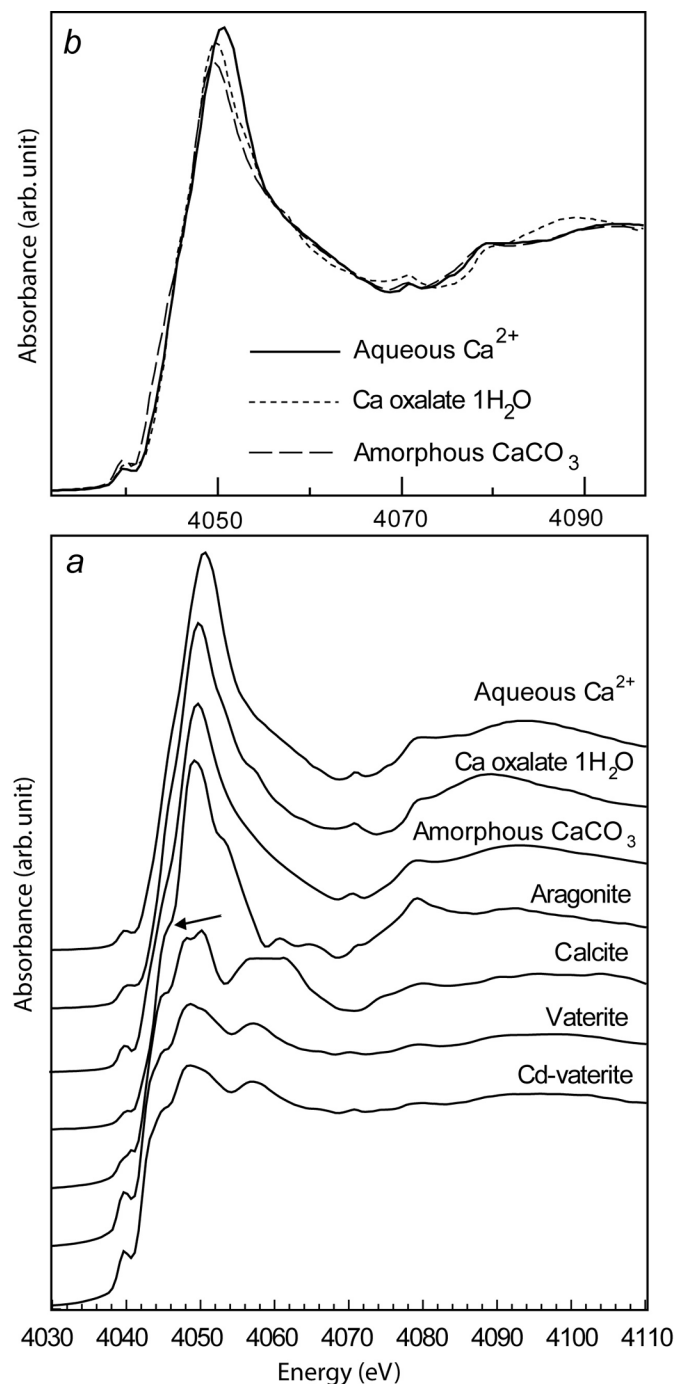
Our previous study using μXRD (3) showed that grain ZnCa3 contained substituted calcite and aragonite, grain ZnCa4 contained substituted calcite, and grain Zn2 did not contain crystalline phases. The two-dimensional μXRD patterns for grains ZnCa5 and Zn3 show that the Bragg reflections for these two grains consist of small arcs of Debye–Scherrer rings, indicating that the grains are composed of micrometer size mosaic crystals (Fig. 2*b*). All reflections correspond to substituted calcite, and the major Ca substituent is Zn, based on μXRF (Fig. 2*a*). Note that although Ca is the major element, the Ca Kα peak has a low intensity relative to the Zn Kα peak due to air absorption and the lower fluorescence yield of Ca vs. Zn. The refined unit cell parameters *a* and *c* for grains ZnCa5 and Zn3 were 4.97 and 16.97 Å and 4.95 and 16.83 Å, respectively, compared with 4.9896 and 17.0610 Å for pure calcite. The cal-

culated formulae using the Vegard law were $Ca_{0.95}Zn_{0.05}CO_3$ and $Ca_{0.89}Zn_{0.11}CO_3$, respectively. The difference in the Zn stoichiometry coefficient obtained using parameters *a* and *c* was ±0.01. The μXRD results for the Cd-containing grains will be presented separately together with Cd L_{III}-XANES data (Isaure et al., manuscript in preparation). Briefly, the grains CdCa2 and Cd10 contain micrometer-sized crystals of substituted calcite and finer (nanometer-sized) crystals of substituted vaterite. Grain CdCa3 contains nanocrystals of substituted vaterite only. Finally, no crystalline phases were detected in grain CdCa6. For Cd-substituted calcite, the Vegard law provides an imprecise estimation of Cd stoichiometry because the contrast in ionic radius between Cd and Ca is small (0.95 Å for Cd^{2+} and 1.00 Å for Ca^{2+} compared with 0.74 Å for Zn^{2+}) (13). For instance, the substitution rate for grain CdCa2 could be anywhere between 30% and 80%. It was not possible to calculate the stoichiometry of Cd in vaterite because of the absence of a Cd end member (see the Experimental section).

Since calcium is the major element in the grains, Ca K-edge μXANES spectroscopy was then performed to get some insight on the composition of the grains and test for the presence of amorphous Ca phases. Fig. 3*a* shows the XANES spectra for several Ca reference compounds. The four $CaCO_3$ species (calcite, vaterite, aragonite, and amorphous $CaCO_3$ (ACC)) have clearly distinct spectra, which enables their identification (14, 15). However, Ca XANES has no sensitivity to substitutional impurities, as seen for instance for low Cd-containing vaterite (Cd content lower than 1%, as estimated by μXRF) and pure vaterite, exhibiting nearly identical spectra. The spectra for aq. Ca^{2+}, Ca oxalate monohydrate, and ACC share some similarities. However, the lower part of the edge is shifted to lower energy for the ACC spectrum, and the maximum of the white line (zero value of the first derivative) increases from 4049.5 (ACC) to 4049.9 eV (Ca oxalate monohydrate), and to 4050.5 eV (aq. Ca^{2+}, Fig. 3*b*). The aragonite spectrum is distinct from the three previous spectra in displaying a shoulder at 4046 eV (arrow in Fig. 3) and a minimum between 4060 and 4070 eV.
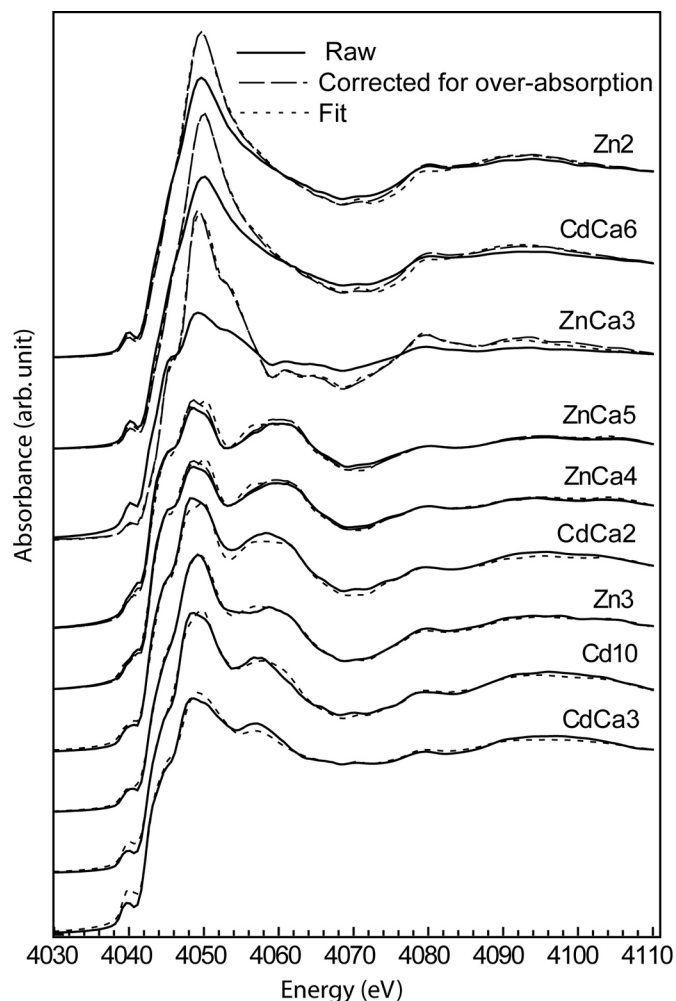
Fig. 4 shows the Ca μXANES spectra for the grains. They were fitted by LC using the standard spectra presented earlier, and the results are presented in Table 2. The ZnCa3 spectrum presents strong similarities with the aragonite

Fig. 3. (*a*) Ca K-edge XANES spectra for the reference compounds used in the linear combination fits and (*b*) enlargement of the main peaks for aq. Ca2+, Ca oxalate monohydrate, and ACC.

Fig. 4. Ca K-edge μXANES spectra for the tobacco grains and corresponding linear combination fits. Five spectra (Zn2, CdCa6, ZnCa3, ZnCa5, and ZnCa4) were corrected for over-absorption.

parameter *a* value found (1.38) corresponds to a very strong over-absorption effect. The fit was not improved significantly by introducing a second component (*NSS* decreased by less than 10%). Thus, the spot analyzed by μXANES likely contains aragonite as the sole Ca species.

The grains ZnCa4 and ZnCa5 were fitted with 98% calcite. The fit was slightly improved with a correction for over-absorption (*NSS* = 0.015% and 0.021%, compared with 0.020% and 0.035%, respectively), and the proportions were unchanged. Adding a second component did not significantly improve the fits (*NSS* decreased by less than 10%).

For grains Zn2 and CdCa6, fits without over-absorption correction were not satisfactory (*NSS* = 0.048% and 0.091%, respectively, for two-component fits). Fair one-component fits with over-absorption correction were obtained with ACC (*NSS* = 0.021% and 0.024%, respectively), but the match was not optimal for the first oscillation (around 4080 eV). Ca oxalate monohydrate and aq. Ca^{2+} provided weaker fits (*NSS* = 0.086% and 0.053% for Zn2, and 0.076% and 0.043% for CdCa6, respectively). Adding a second component did improve the reproduction of the first oscillation. Several fits of equivalent qualities were obtained with ACC

spectrum but with markedly lower amplitude. The drop in amplitude suggests some over-absorption effect (12) due to a high Ca content of the analyzed spot. The fit without over-absorption correction (see the Materials section) did not provide a satisfactory result (*NSS* = 0.065% with 68% vaterite and 25% aragonite). Introducing an over-absorption correction greatly improved the fit (Fig. 4, *NSS* = 0.014% with aragonite as the only component). The over-absorption

Table 2. Ca µXANES results.

Treatment	Grain name	a^a	Proportion of Ca species determined by linear combination fitting of the µXANES spectra (%)						Sum	NSS (%)^b
			Calcite	Vaterite	Aragonite	Amorphous CaCO$_3$	Aq. Ca^{2+}	Ca oxalate 1 H$_2$O		
Zn + Ca	ZnCa3	1.38			97±2				97	0.014^c
	ZnCa4	0.12	98±2						98	0.015^c
	ZnCa5	0.17	98±2						98	0.021^c
Zn	Zn2	0.27			22±10	76±15			97	0.011^c
		0.27				77±15		20±15	97	0.016
		0.27				79±15	17±15		96	0.019
		0.42				(excluded)	55±15	45±15	100	0.050
	Zn3		62±5			29±5			91	0.009^c
			70±5					22±5	92	0.016
			71±5				21±5		92	0.018
Cd+Ca	CdCa2		85±5			13±5			98	0.012^c
			87±5					10±5	97	0.014
			89±5				9±5		98	0.015
	CdCa3			77±5		21±7			98	0.031^c
				79±5				20±7	99	0.036
				82±5			16±7		98	0.037
	CdCa6	0.38				74±15		25±15	99	0.015^c
		0.42				68±15	32±15		100	0.019
		0.28				(excluded)	73±15	25±15	98	0.040
Cd	Cd10		29±7	42±8			25±5		96	0.022^c
			25±7	37±8		34±5			96	0.025
			28±7	42±8				26±5	96	0.028

^{a}Coefficient of over-absorption.

^{b}Residual between fit and experimental data $NSS = \sum(\mu_{experimental} - \mu_{fit})^2 / \sum(\mu_{experimental})^2 \times 100$ in the 4000–4150 eV range, where µ is the normalized absorbance.

^{c}Fit shown in Fig. 4. The error bars on the percentages correspond to the variation needed to increase NSS by 20%.

as a major component (about 80% and 70% of total Ca) and various species as secondary components. *NSS* values were more than doubled if ACC was excluded (Table 2 and Fig. 1 in the Supplementary information).[3] Therefore, grains Zn2 and CdCa6 likely contain ACC as major species and an additional species whose nature remains unknown.

For the other grains (Zn3, CdCa2, CdCa3, and Cd10), over-absorption correction did not improve the fits. Calcite was the major form in grains Zn3 and CdCa2, and fits of equivalent quality were obtained with ACC, aq. Ca^{2+}, and Ca oxalate monohydrate as minor species. Aqueous Ca^{2+} is unlikely in solid-state material. ACC and Ca oxalate monohydrate are more likely. In the absence of reference spectra for Ca bound to organic ligands other than oxalate, this latter compound may be considered as a proxy for Ca bound to organic compounds in general. Therefore, this pool is referred to as organic Ca and (or) ACC in Table 3. Vaterite was found in grains CdCa3 and Cd10. For this latter grain only, no satisfactory fit was obtained with two components (*NSS* = 0.046%), so a third component was introduced. Again, a contribution of organic Ca and (or) ACC was found in grains CdCa3 and Cd10.

The speciation of Ca was then compared with the mineralogy and morphology of the grains (Table 3). The percent-

ages were rounded to the nearest ten for clarity. Except for two grains, ZnCa3 and CdCa2, the same crystalline species were identified by µXRD and Ca µXANES. Zn-substituted calcite and Cd-substituted vaterite were identified by µXRD in grains ZnCa3 and CdCa2, respectively, but not by Ca µXANES spectroscopy. This difference likely results from the larger beam size and higher penetration depth of X-rays in µXRD measurements relative to µXANES (16 × 7 µm vs. 5 × 5 µm and a few tens of µm at 17 keV vs. a few µm at 4 keV). Thus, µXRD probes a different material volume than Ca µXANES, even when conducted on the same spot.

Discussion and conclusion

Results showed that besides crystalline calcium carbonates (calcite, vaterite, and aragonite), the tobacco grains contained ACC as well. Whewellite (Ca oxalate monohydrate) did show up in some XANES fits, but its presence could not be firmly attested. Ca oxalate mono- and dehydrate have several XRD peaks in common with calcite but several peaks at distinct positions as well. These two minerals were positively identified by µXRD in other tobacco grains based on the presence of these specific peaks (3). In the present

Table 3. Summary of the information obtained on each grain.

Treatment	Grain name	Ca speciation (μXANES results)[1]	Mineralogy (μXRD results)	Aspect of the grain (SEM results)
Zn + Ca	ZnCa3	100% aragonite	Aragonite, Zn-subst. calcite ($Ca_{0.93}Zn_{0.07}CO_3$)	Faceted
	ZnCa4	100% calcite	Zn-subst. calcite ($Ca_{0.87}Zn_{0.13}CO_3$)	Faceted
	ZnCa5	100% calcite	Zn-subst. calcite ($Ca_{0.95}Zn_{0.05}CO_3$)	Not observed
Zn	Zn2	80% ACC, 20% undetermined	No diffraction peaks	Rounded
	Zn3	70% calcite, 30% organic Ca, and (or) ACC	Zn-subst. calcite ($Ca_{0.89}Zn_{0.11}CO_3$)	Not observed
Cd + Ca	CdCa2	90% calcite, 10% organic Ca, and (or) ACC	Cd-subst. calcite, Cd-subst. vaterite	Not observed
	CdCa3	80% vaterite, 20% organic Ca, and (or) ACC	Cd-subst. vaterite	Rounded
	CdCa6	70% ACC, 30% undetermined	No diffraction peaks	Not observed
Cd	Cd10	30% calcite, 40% vaterite, 30% organic Ca, and (or) ACC	Cd-subst. calcite, Cd-subst. vaterite	Rounded and faceted

Note: The error bar on the percentages varies from 5% to 15% depending on the species (see Table 2).

study, no such peaks were found on the XRD patterns. However, it is still possible that coarse crystals of Ca oxalate mono- or dehydrate are present but produce nonspecific peaks only, or that Bragg conditions were not met for these coarse crystals. Therefore, the presence of Ca oxalate mono- and dehydrate cannot be ruled out. Other undetermined organic ligands may also complex Ca. In addition, mixed mineral and organic Ca compounds such as organic matter containing calcite (16) may occur.

The Ca μXANES analysis showed that strong over-absorption effects may take place and decrease dramatically the amplitude of the spectra. We show that this effect is far from negligible when identifying and quantifying Ca species. For instance, for grain ZnCa3, the uncorrected spectrum was fitted by 68% vaterite and 25% aragonite, and the corrected spectrum was fitted with 100% aragonite. Note that the LC fit without over-absorption correction was relatively bad, which alerted us on the possibility of an over-absorption effect.

In the environment, ACC is thermodynamically unstable and rapidly transforms into vaterite and then calcite (17). However, it is found as a stable compound in plants (e.g., cystoliths) and animals (e.g., cuticle of crustaceans, spicules of ascidiae, granules in molluscs) (18). ACC is probably stabilized by proteins, magnesium, and phosphorus in these organisms (18). In our case, Mg and P were found in the grains.

Biologically controlled biomineralization leads to well-defined mineral species and shapes. Here, the variety of morphologies and of $CaCO_3$ crystal structures, and their co-existence with amorphous and possibly organic forms, supports the hypothesis of a biologically induced (as opposed to biologically controlled) biomineralization. This study illustrates the potential of microfocused X-ray techniques to study biomineralization processes, and strategies of metals immobilization developed by plants to cope with metal toxicity.

References

1. Y.E. Choi, E. Harada, M. Wada, H. Tsuboi, Y. Morita, T. Kusano, and H. Sano. Planta, **213**, 45 (2001).
2. Y.E. Choi, E. Harada, G.H. Kim, E.S. Yoon, and H.J. Sano. Plant Biol. **47**, 75 (2004).
3. G. Sarret, E. Harada, Y.E. Choi, M.P. Isaure, N. Geoffroy, M. Birschwilks, S. Clemens, S. Fakra, M.A. Marcus, and A. Manceau. Plant Physiol. **141**, 1021 (2006).
4. H. Lowenstam and S. Weiner. *In* On biomineralization. Oxford University Press, Oxford, UK. 1989.
5. Y.E. Choi and E. Harada. Plant Biol. **48**, 113 (2005).
6. J. Paquette and R.J. Reeder. Geochim. Cosmochim. Acta, **59**, 735 (1995).
7. R.J. Reeder. Geochim. Cosmochim. Acta, **60**, 1543 (1996).
8. Y. Politi, Y. Levi-Kalisman, S. Raz, F. Wilt, L. Addadi, S. Weiner, and I. Sagi. Adv. Funct. Mater. **16**, 1289 (2006).
9. M.A. Marcus, A.A. MacDowell, R. Celestre, A. Manceau, T. Miller, H.A. Padmore, and R.E.J. Sublett. Synchrotron Radiat. **11**, 239 (2004).
10. A. West. Solid state chemistry and its applications. Wiley, New York. 1984.
11. T.J. Ressler. J. Phys. IV, **7**, c2–269 (1997).
12. A. Manceau, M.A. Marcus, and N. Tamura. *In* Applications of synchrotron radiation in low-temperature geochemistry and

rnvironmental science. *Edited by* P. Fenter, M. Rivers, N. Sturchio, and S. Sutton. Mineralogical Society of America, Washington, DC. 2002. pp. 341–428.

13. R.D. Shannon. Acta Crystallogr. A, **32**, 751 (1976).

14. Y. Levi-Kalisman, S. Raz, S. Weiner, L. Addadi, and I. Sagi. Adv. Funct. Mater. **12**, 43 (2002).

15. S. Pattanaik. Nucl. Instrum. Methods Phys. Res., Sect. B, **229**, 367 (2005).

16. B.L. Phillips, Y.J. Lee, and R.J. Reeder. Environ. Sci. Technol. **39**, 4533 (2005).

17. T. Ogino, T. Suzuki, and K.J. Sawada. Cryst. Growth, **100**, 159 (1990).

18. S. Weiner, Y. Levi-Kalisman, S. Raz, and L. Addadi. Connect. Tissue Res. **44**(Suppl. 1), 214 (2003).